Journal of Vibration Engineering & Technologies (2018) 6:249–260
https://doi.org/10.1007/s42417-018-0032-5

ORIGINAL PAPER

Probabilistic Diagnostic Algorithm-Based Damage Detection for Plates with Non-uniform Sections Using the Improved Weight Function

非均匀截面

Jingjing Zhao[1] · Xiaoting Miao[2] · Fucai Li[1] · Hongguang Li[1]

Received: 14 June 2016 / Revised: 22 June 2016 / Accepted: 28 July 2016 / Published online: 17 August 2018

Abstract

Introduction The current studies on damage detection based on guided wave mainly focus on uniform-section plate-like structures. However, plates with non-uniform sections are also essential structures in some engineering applications, such as ships, bridges, aircraft, and buildings. It is essential to identify damage in the non-uniform-section plates (NUSPs).

Objectives An improvement is put forward to make reconstruction algorithm for the probability inspection of damage (RAPID) feasible on NUSPs.

Methods Reconstruction algorithm for the probability inspection of damage (RAPID) is a promising kind of tomography technique for detection and supervising of structures. The damage signatures based on the differences between the Lamb wave signals captured from the undamaged (reference) and damaged (present) states are used to assess the probability of the damage. The elliptical weight function commonly used in the RAPID algorithm limits the applications of the method in identifying damage in non-uniform-section plates. In this study, a novel method is proposed to choose the weight function that satisfies not only uniform-section plates but also NUSPs. A series of experiments on aluminum plates are carried out to validate the correctness of the method mentioned before.

Conclusion The results indicate that the improvement considerably increases the precision of the localization of damage in NUSPs.

Keywords Structural health monitoring · Probability-based diagnostic image · Damage identification · Non-uniform-section plates

Introduction

Shell structures and thin plates have been widely applied in industries. The structures and plates are prone to develop cracks and material losses due to impact loads and fatigue during manufacturing as well as in-service events. Cracks and material loss usually are not visible which could lead to sudden failure of the entire structure. Since it is not easy to detect the hidden damages in structures by the traditional ways, the real-time structural health monitoring (SHM) techniques, which are widely used in the field of aerospace, shipping and civil engineering [1, 2], have been intensively investigated.

As one of the most promising methods, Lamb wave tomography techniques have attracted considerable attention for the purpose of SHM [3–6], while having a great advantage of excellent propagation capability as well as high sensitivity measuring the variation of target's properties [7]. With the features of lamb waves, tomography techniques developed from medical science were introduced in SHM to provide considerable ways to detect the defects in structures in recent years. The implementation with tomography techniques can obtain intuitional quantitative images to detect defects. The locations and sizes of damage were reconstructed and highlighted in the images. Most of the tomography techniques are derived from the time-of-flight (ToF) theory which is calculated from the reflected waves or transmitted waves [4, 6, 7]. Many studies demonstrate the feasibility of the tomography techniques based on ToF.

✉ Jingjing Zhao
zjj316@sjtu.edu.cn

Fucai Li
fcli@sjtu.edu.cn

[1] State Key Laboratory of Mechanical System and Vibration, Shanghai Jiao Tong University, Shanghai 200240, China

[2] Shanghai Electro-Mechanical Engineering Institute, Shanghai 201109, China

Leonard and Hinders et al. [3] applied the Lamb wave tomography technique on pipes and pipe-like structures, and the tomographic images based on ToF were obtained with the presence of a flaw. Jansen and Hutchins [4] utilized immersion techniques to reconstruct damage images in metallic samples. The results provided enough information for locating the defects and figuring out nature of the defects. The phased-array pulse-echo approach was used by Giurgiutiu and Bao to build diagnostic image [5]. Lin and Yuan [6] demonstrated the migration technique to interpret the waves that reflected from the damage and then imaged the damage in geophysical area. Rao [8] uses transient dynamic respond to estimate the damage in circumstances. However, identifying the damage signatures among massive response-wave signals is challenging. Due to the dispersion characteristic and multiple modes, there are different modes and propagation velocities of Lamb wave with the same frequency. Meanwhile, multimode conversion occurs in reflected waves or transmitted waves when the waves reach edges or defects on structures.

Many efforts have been endeavored to develop a tomographic technique which weakens the influence of complicate response-wave signals. There was no significant breakthrough until Hay and Royer [9] introduced an algorithm called reconstruction algorithm for probabilistic inspection of damage (RAPID) in the field of damage identification. This algorithm uses an intuitional image to show the probability of the existence of damage in an area marked by an active sensor network. In RAPID algorithm, an important parameter called signal difference coefficient (SDC) is obtained by comparing the variation of signals between the undamaged and damaged states from individual sensing paths. The results from the study [9] demonstrated that RAPID algorithm has high sensitive to the material loss and was rare impressible to noise and complex structures. Zhao [10, 11] utilized the RAPID algorithm to reconstruct the defect distribution probability map on an aircraft wing for health monitoring. The effect of the algorithm was verified through simulating the types and stages of the defect. Furthermore, Zhao [12] compared several tomography techniques including the filtered back projection algorithm, the algebraic reconstruction technique, and RAPID algorithm, and then summarized that RAPID algorithm had the flexibility in array geometry selection to reconstruct images with good quality in a completely automated way. Meanwhile, some innovations were brought into the RAPID algorithm to improve its performance. Koduru [13] inspected the corrosion in the steel plate overcoming the influence arising from anisotropic liquid loading on the structure with the RAPID algorithm integrated with selected mode of exciting waves. Zhang [14] has discussed the effectiveness of the correlation function of signals to prove that the correlation function can detect damage even noise exists. Therefore, SDC can be used to distinguish the signals in the undamaged and damaged states. Wang [15–17] introduced Shannon entropy and digital damage fingerprints (DDFs) to highlight the variation in signals induced by the existence of damage. In addition, he proposed an idea called virtual sensing paths to reduce negligence of the blind zones. Furthermore, the influence factors in the RAPID algorithm were deeply studied to get images that are more precise. Sheen [18] assessed the influence of the elliptical effective area which depends on the selection of the scaling parameter β. A reasonable choice of β limited the deviation of the damage between -5% and 5%. Wu [19] clarified the influences of various factors used in the RAPID algorithm in detail, including the selection of the damage index and frequency, the network of sensing paths, and the size of effective area. The sensor array network constituted by seven sensors was the best choice for damage detection in the airfoil as the results from the coverage rate and the redundancy requirements [20]. The optimal sensor network was installed on the horizontal tail for full-scale monitoring, forming an efficient diagnostic map. Then, an approach was presented to optimize the network and the scaling parameter, β. Zeng [21] developed a strategy of selecting the length of data to gain a high resolution. The length of data is closely related to SDC and β, and then affects the accuracy of the defect location. All these studies used the RAPID algorithm to identify the damage in uniform-section plates or in uniform structures with stiffeners without considering the influence of thickness change. However, plates with non-uniform sections are also key structures in some engineering applications, like the tube–tube sheet junction of a heat exchanger and the lap shear joint of layers in an aircraft fuselage. Waves propagating in plates with continuous varying thickness are also an important widespread issue in industries. Moreover, a failure would occur more easily in the place where the thickness varies due to its high concentration. Therefore, the change of plate sections should be considered.

In general, a guided wave propagating in a plate with variable thickness is much more complex than in one with uniform thickness resulting from the multimode conversion processes due to thickness variation. The hybrid boundary element method was adopted by Younho Cho [22] to simulate the process of wave propagation in a step discontinuity plate. When a new cut-off mode appeared, the remarkable mode conversion occurred during the guided waves propagating. The study of El-Kettani [23] indicated that an appointed guided wave would reach its cutoff due to the decrease of the thickness. The performance of guided waves containing a Gaussian section variation when propagating in plates has been proposed by Marical [24], and a theory of energy balance has been developed. It is difficult to identify damage in the non-uniform-section plates (NUSPs) due to the conversion of wave modes. The tomography techniques

厚度改变引起导播模态转换

mentioned above are only used in the uniform-section plates. Therefore, it is worth taking attention to obtain tomographic images with an easy and convenient method in NUSPs.

To get tomographic images with high quality and precision in NUSPs, the influence of non-uniform section in plate structures should be considered. A novel strategy to extend the application of the RAPID algorithm is first proposed to choose the weight function satisfying not only uniform-section plates but also NUSPs. Then, the self-adapting weight function method is established to better detect the defects in the NUSPs. The rest of this paper is arranged as follows. The section "Lamb Wave Propagation in NUSP" briefly specifies the basic properties of Lamb wave propagation. In section "Tomography Algorithm", the conventional RAPID algorithms improved about choosing the weight function. In section "Procedure of Finite-Element Analysis", the new method and the conventional one are compared using finite-element analysis. The experimental setup is introduced in the next section. In section "Experiment", the effect and accuracy of the reconstructed image are addressed by comparing the results of from the conventional and improved RAPID algorithm. Finally, conclusions are drawn in section "Conclusions".

Lamb Wave Propagation in NUSP

Lamb Wave Propagation in Plate Structures

A Lamb wave is a category of elastic waves propagating in thin plates and shell structures. Based on Helmholtz decomposition, both the in-plane and out-off plane displacements are acquired under the plate stain condition. The Rayleigh–Lamb wave equations can describe the features of frequency dispersion [1, 7]:

Symmetric mode：

$$\frac{\tan(qh)}{\tan(ph)} = -\frac{4k^2pq}{(q^2-k^2)^2} \tag{1}$$

Anti - symmetric mode:

$$\frac{\tan(qh)}{\tan(ph)} = -\frac{(q^2-k^2)^2}{4k^2pq}, \tag{2}$$

where $p^2=(\omega/c_L)^2-k^2$; $q^2=(\omega/c_T)^2-k^2$; ω is the wave's circular frequency; k ($k=\omega/c_p$) is the wave number; c_p is the phase velocity of the Lamb waves.

Lamb wave dispersion curves describe the relationship between the velocity and the frequency. There is more than one value of k satisfying Eqs. (1) and (2) when ω is determined. f ($f=\omega/2\pi$) represents the frequency of the wave. The group velocity c_g is calculated by the derivative of ω with respect to k. Then, the Lamb wave dispersion curves can be achieved. In this paper, aluminum alloy is used as experiment material. Material properties of alloy are listed in Table 1. The dispersion curves are shown in Fig. 1.

The description of Lamb wave in an isotropic and homogenous plate can be split into two parts based on the direction of particle motion denoted as S_i and A_i, respectively. The subscript i denote the wave order starting from 0. S_i modes predominantly have radial in-plane displacement of particles, while A_i modes have out-of-plane displacement [7]. From Fig. 1, Lamb wave dispersion curves consist of multiple propagation modes. The velocity, including the phase velocity and the group velocity, changes with the frequency-thickness product (f·d), which results in multimode and dispersion effect.

To simplify Lamb wave signals, two issues must be considered. First, the wave mode has to be carefully selected. Before the cutoff of A_1 mode, there are only S_0 and A_0 mode. Therefore, the basic mode should be chosen to avoid the effect of multimode. Second, the selection of the Lamb wave mode is also an essential step in damage detection. The selection of narrowband signals can decrease the influence of dispersion. In this study, S_0 mode has faster propagation velocity than A_0 mode, which is selected damage detection. It takes less time for S_0 mode than A_0 mode to propagate through the same distance. Thus, there are fewer reflected waves in the response waves. The influence of reflected wave decreases.

Time-of-Flight of Lamb Waves in Aluminum NUSP

ToF is the time lag between the wave's generation in the actuator and its capturing in the sensor. Due to the effect of dispersion, the phase velocity changes with the frequency–thickness products (f·d). Therefore, a special method must be introduced to calculate ToF in NUSPs.

Assume that the bottom surface of the aluminum NUSP is flat. A 3D Cartesian coordinate system is used in the network. The surface is placed on the x–y plane, as shown in Fig. 2. Any point on the plate (plane) can be described by its coordinate (x_i, y_i). Meanwhile, assume that the top surface can be described as $d_i=z_{top}$ (x_i, y_i) where z_{top} (x_i, y_i) represents the thickness function of the NUSP. Therefore, the phase velocity at (x_i, y_i) can be indicated as $v_p(f{\cdot}d_i)$. The method of calculating ToF between any two points on the plane is introduced as follows.

First, the bottom surface of the aluminum plate is meshed with small uniformly distributed grids as the datum plate. Two points denoted as $P(x_p, y_p)$ and $Q(x_q, y_q)$ are chosen in the

Table 1 Material properties of alloy

Poisson's ratio	0.33
Density (kg/m^3)	2700
Young's modulus (GPa)	71

频散曲线

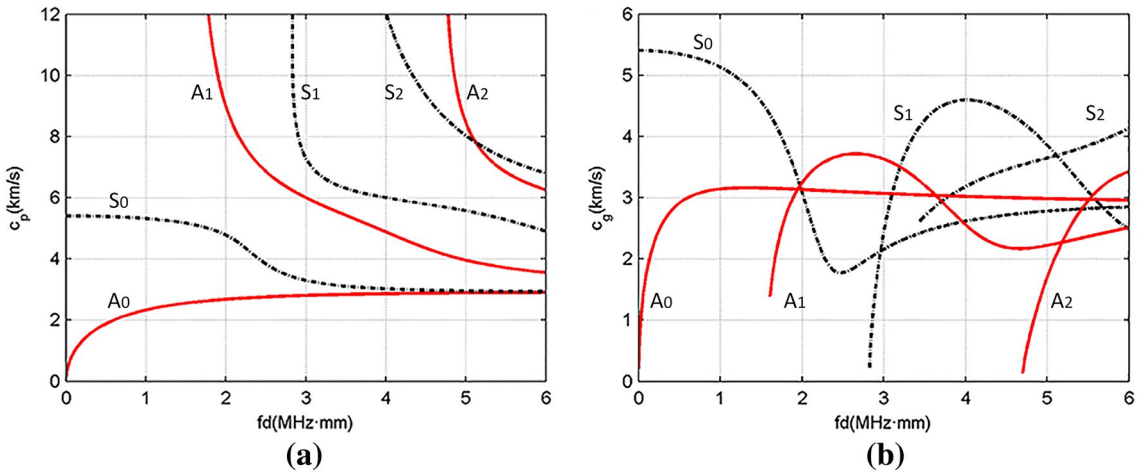

Fig. 1 Lamb wave dispersion curves of alloy. **a** Phase velocity dispersion; **b** group velocity dispersion

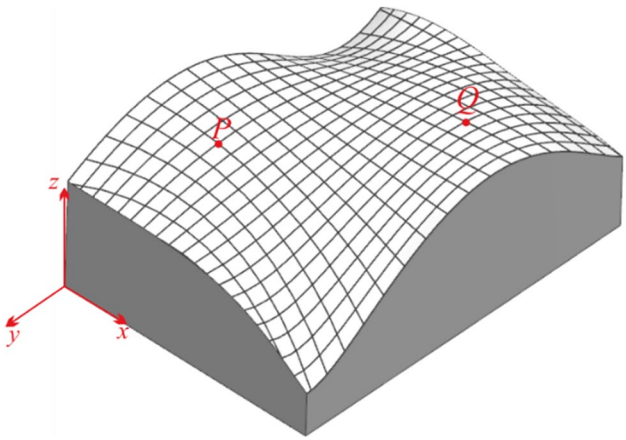

Fig. 2 NUSP with the thickness function of z_{top} (x_i, y_i)

coordinate system. The distance between two specified point $P(x_p, y_p)$ and $Q(x_q, y_q)$ can be expressed as follows:

$$D_{PQ} = \sqrt{\left(x_p - x_q\right)^2 + \left(y_p - y_q\right)^2}. \tag{3}$$

Second, Line PQ is divided into N isometric sections, length of each DPQ/N. The location of the midpoint of the ith part is denoted as (x_i, y_i). If N is big enough, which implies that the length of each part is so short that the thickness at each part can be regarded as constant. Thereby the group velocity at each part is constant, which can be denoted as $v_p(f{\cdot}d_i)$ for the ith part.

Finally, ToF between grids P and Q is obtained by summing each part:

$$t_{PQ} = \sum t_i = \frac{D_{PQ}}{N} \sum \frac{1}{v_p\left(f \cdot d_i\right)}. \tag{4}$$

Here, t_i denotes the time lap that the wave propagates through the ith part with the constant phase velocity $v_p(f{\cdot}d_i)$. t_{PQ} is the total time taken by the wave propagating through Line PQ.

This approach increases the accuracy of ToF, and because the non-constant thickness is taken into considered, it is more reasonable and practical. The $f{\cdot}d$ of the excitation signal and the maximum of the NUSP should be smaller than the cut-off frequency of A_1 mode to minimize the influence of the multiple modes of the Lamb waves.

Tomography Algorithm

RAPID Algorithm

The RAPID is an algorithm which uses probability to locate the defect. The concept of probability-based approach was brought into the field of damage identification for the first time by Hay [9]. By applying this method to damaged structures, a reconstructed image will be obtained by highlighting the damage using a sensor network. The sensor network consists of sparse sensors, which is installed on the structure.

The monitoring area of the structure is meshed into uniformly distributed grids. For a sensing path, each grid in the effective area has a value to represent the probability of the presence of damage. For any grid in the monitoring area, the probability of the presence of damage is the summation of probability calculated by every sensing path at this position. Then, the center of the identified damage is evaluated by the value of the probability, where highest values denote the most possible position of the damage.

The damage index (DI) and weight functions determine the value of probability in every grid to assess the presence of damage. The DI as a statistic data estimates the change of

进行分段处理

Lamb waves received by sensors under the undamaged and damaged states. It shows the similarity between the signals captured by two states:

$$\mathrm{DI} = \frac{|\mathrm{SDC}_1 - \mathrm{SDC}_2|}{\mathrm{SDC}_1}, \tag{5}$$

where SDC1 and SDC2 are the SDC between the signal achieved by sensor and actuator in undamaged state and damaged state in the same sensing path, respectively. DI equals 0 and 1, corresponding to two conditions of the signals, totally uncorrelated and totally correlated.

The weight function is measured by the positional relationship between the grids and the selected sensing paths. It is assumed that the damage is the sole reason causing the changes of the Lamb wave signals in different states.

As a result, the estimation at position (x, y) can be written as follows [14]:

$$P(x,y) = \sum_{i=1}^{N} P_i(x,y) = \sum_{i=1}^{N} \mathrm{DI}_i \cdot W_i. \tag{6}$$

Here, $P_i(x, y)$ is the probability component derived from the ith sensing path at (x, y). DI_i denotes the DI value of the ith sensing path. W_i is the non-negative weight distribution function of the ith sensing path, which ranges from 0 to 1.

Based on this method, the influences including the complexity of the structural geometry and boundary condition exist in both the undamaged and damaged signals, which do not affect the effectiveness of the RAPID algorithm for locating damage.

The Linear Elliptical Weight Function

Linear elliptical weight function is one type of non-negative linearly decreasing distribution functions, which ranges from 0 to 1. In a pitch-catch sensing pair, the contour of the distribution function consists of a set of ellipses with foci at the positions of the actuator and the sensor, which was discussed by Wang [15]. As the damage can cause the most significant change in the signal when it is on the direct sensing path for a particular sensing path, the value of the weight function should have its maximum on that path. Accordingly, the value of the weight function is determined by the distance between the damage and the direct path of the sensing pair [19]:

$$W_i\left[R_i(x,y)\right] = \begin{cases} 1 - \frac{R_i(x,y)}{\beta}, & R_i(x,y) < \beta \\ 0, & R_i(x,y) \geq \beta \end{cases}, \tag{7}$$

where β is a scaling parameter controlling the size of the effective area. In RAPID algorithm, the shape of the effective area for each sensing path is an ellipse. Artifacts will be introduced if β is too small, and resolution will be lost if β is too large [10].

β的取值影响

$R_i(x, y)$ is defined as the relative distance from (x, y) to the ith sensing path:

$$R_i(x,y) = \frac{D_{a,i}(x,y) + D_{s,i}(x,y)}{D_i} - 1, \tag{8}$$

where D_i is the direct distance between the actuator and the sensor of the ith sensing path. For the same sensing path, $D_{a,i}(x, y)$ is the distance from the actuator to the point (x, y), while $D_{s,i}(x, y)$ is the distance from the point (x, y) to the sensor, as shown in Fig. 3.

The appointed scaling parameter β and D_i determine the maximum length of each sensing path, and then determine the length of signals used to calculate the SDC. The signals start at T_0:

$$T_0 = \frac{\beta \cdot D_i}{c_{\mathrm{pmax}}}, \tag{9}$$

where c_{pmax} is the maximum phase velocity in the sensing path in the NUSP.

The signals end at T_t:

$$T_t = \frac{\beta \cdot D_i}{c_{\mathrm{pmin}}} + \frac{T_{\mathrm{in}}}{2}, \tag{10}$$

where c_{pmin} is the minimum phase velocity in the sensing path in the UNSP. T_{in} is the time duration of the excitation signal [19].

The Structural Weight Function

As aforementioned, the RAPID algorithm using the elliptical weight function applies to the plate with uniform sections [10, 18, 19]. In uniform-section plates, the phase velocity (c_{p}) of the selected mode remains constant for the whole plates. Therefore, the shape of the weight function is assumed to be the contour of a set of ellipses with the location of the actuators and sensors as the ellipse foci,

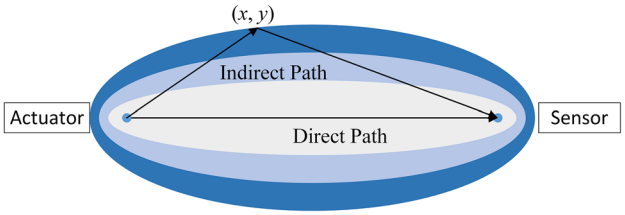

Fig. 3 Illustration of the elliptical distribution function of the RAPID algorithm

such that the relative path length is the same on each contour. However, there are various plates with non-uniform sections in practice. In this situation, the elliptical weight function does not satisfy to demonstrate the effective area of a sensing path in non-uniform-section plates (NUSPs), because c_p is not constant value all the time. When c_p is not a constant value for NUSP due to vary thickness, the elliptical assumption does not stand any more. Therefore, the RAPID algorithm is in need of an improvement to be adapted to the situations of NUSPs.

The most distinction between NUSPs and uniform-section plates is the phenomenon that plates have continue or discontinue variation of thickness. In other words, the situation that c_p is a constant value is a particular case. To apply RAPID algorithm on NUSPS and obtain reconstructed images with high resolution, the change of thickness and the shape of the effective area have to be taken into consideration. When Lamb wave propagates from the actuator, through the weight function contour, to the sensor, the value of c_p keeps changing all the time. According to this phenomenon, the weight function has to be altered to couple with the change of c_p. The altered weight function for ith sensing pair is denoted as $W_i[B_i(x, y)]$ called structural weight function. The definition of $W_i[B_i(x, y)]$ is given by the following:

$$W_i\left[B_i(x,y)\right] = \begin{cases} 1 - \frac{B_i(x,y)}{\alpha} & B_i(x,y) < \alpha \\ 0 & B_i(x,y) \geq \alpha \end{cases}, \tag{11}$$

where

$$B_i(x,y) = \frac{t_{a,s}(x,y) - t_i}{t_i} \tag{12}$$

$$\frac{D_{a,i}(x,y)}{c_{p,a}} + \frac{D_{s,i}(x,y)}{c_{p,s}} = t_{a,i}(x,y) + t_{s,i}(x,y) = t_{a,s}(x,y). \tag{13}$$

In the equations above, α is a scaling parameter that controls the range of the effective area. Similar to that of β, the selection of α must correspond to the length of the measurement data [21]. t_i is the time lag calculated using Eq. (4), when the wave propagates directly from the actuator to the sensor for the ith sensing path. $B_i(x, y)$ denotes the relative time for the wave to propagate from the actuator to the sensor through the grid (x, y), related to $t_{a,s}(x, y)$ and t_i. When the grid (x, y) is on the sensing path, the value of B_i is at its minimum, 1, and $W_i[B_i(x, y)]$ equals maximum, 1, at the same time. The ToF of indirect and direct paths determines the value of B_i. When the ToFs are the same at different grids, the values of $W_i[B_i(x, y)]$ are also the same. Therefore, the structural weight functions reflect the shapes of NUSPs and the distance of the indirect paths.

最小值 0

Figure 4 shows the structural weight function of a trapezoidal plate for instance. The location of the grid M is picked as actuator, while the location of the grid N is picked as sensor. The set of the structural weight function contours are calculated from Eqs. (11)–(13). Figure 4b is the structural weight function contours of basic symmetric mode S_0; Fig. 4c is the structural weight function contours of basic anti-symmetric mode A_0. In Fig. 4, the contours of the structural weight function are no longer ellipse. Therefore, it is necessary to using the structural weight function instead of the linear elliptical weight function into the RAPID algorithm for detecting damage in NUSPs.

Procedure of Finite-Element Analysis

Procedure of the Ramp Aluminum Plate Model

To validate the accuracy of the improved RAPID algorithm, a finite-element (FE) analysis is carried out towards a ramp aluminum plate which is the simplest and most typical NUSPs and widely used structure. The ramp plate has a flat-bottom surface. The curve of the top surface in the ramp plate matches a function, which is linear in this example. The FE results obtained from the improved RAPID algorithm are compared with those from the conventional algorithm to validate the former one.

Finite-element analysis is conducted to investigate the Lamb wave signals propagating in a ramp aluminum plate and to locate a hole (the circular hole with the radius is 5 mm). To make the comparison clear, this paper applies the two algorithms on the aluminum NUSP. A ramp aluminum plate (650 mm × 650 mm) with continuously varying thickness is studied, which is presented in detail in Fig. 5a. In addition, the monitoring area of the ramp plate is 450 mm × 450 mm, with 12 sensors placed in Fig. 5b. The thickness of the plate linearly decreases from 7.5 mm at the bottom ($y = 0$) to 3 mm at the top of plate ($y = 450$ mm). The hole locates at (270, 180) according to the system. The model is built using three-dimensional elements. The dynamic simulation of Lamb wave activation and acquisition is accomplished using ABAQUS/Explicit. The model of the plate is meshed using eight-node three-dimensional linear brick elements (C3D8R). The element size of C3D8R in the plate is set as 1 mm and four layers are modeled in the thickness direction. A hole is simulated by removing the equivalent elements. The material properties of alloy are present in Table 1. The central frequency of the excitation signal is 210 kHz with seven-cycle sinusoidal tone burst enclosed in a Hanning window, which is imposed as a shear force on the simulated actuator along the radial direction. The sampling rate is 100 MHz.

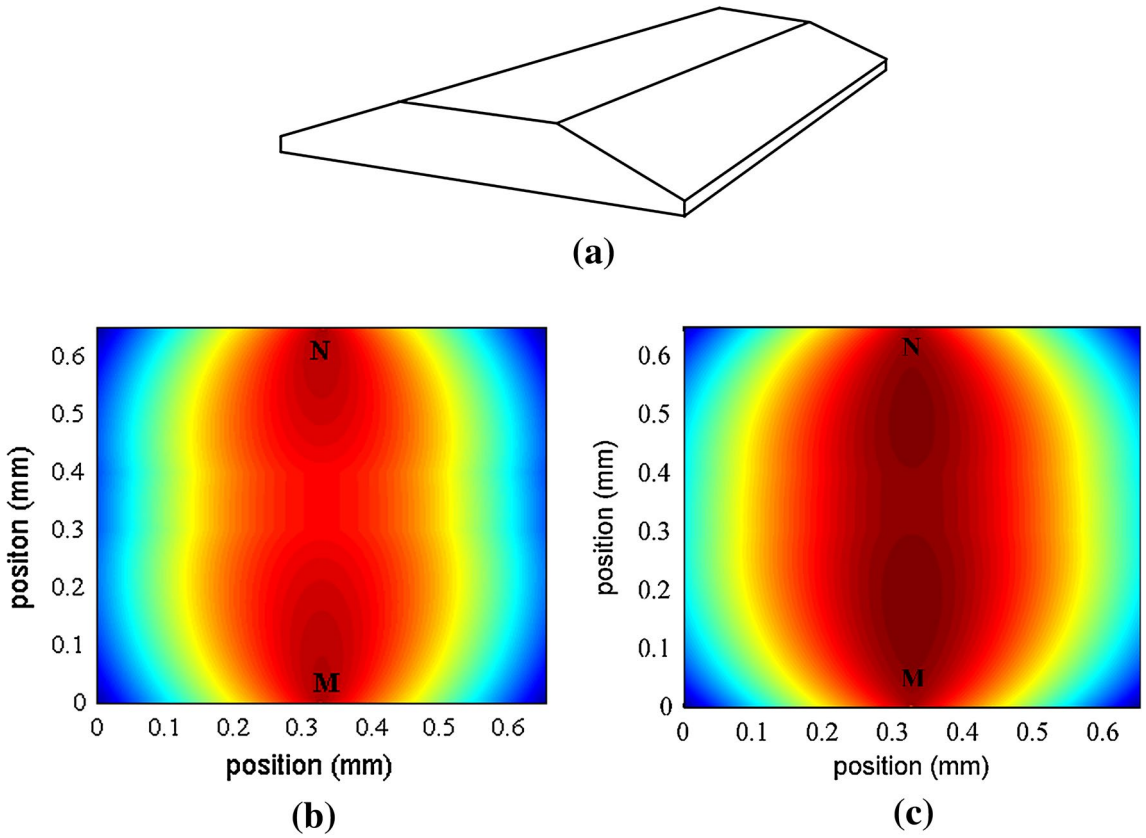

Fig. 4 Contours of the structural weight function in a trapezoidal plate: **a** is the trapezoidal plate; **b**, **c** is the contours based on S_0 mode and A_0 mode, respectively

Procedure of RAPID Algorithm Using the Structural Weight Function

The procedure of improved RAPID for defect identification is summarized as the following four steps.

1. One PZT is selected as the actuator, while several other PZTs as sensors. An actuator and a sensor consist a pitch-catch sensing path to capture signals in both the undamaged and damaged states. There are 56 sensing paths building up the network shown in Fig. 5b. Calculate SDC and DI values of each sensing path with this actuator using the basic symmetric mode S_0.
2. Then, 12 PZTs as actuators excite in turn until all the 56 SDC and DI values are obtained.
3. Reconstruct the images using Eqs. (5)–(6) and Eqs. (11)–(13).

Results and Discussion of Simulation

RAPID algorithms with the linear elliptical weight function or the structural weight function are both applied in simulations. The images of the different kinds of weight functions for the ramp plate without damage are building up on the basis of Eq. (7) and Eq. (11). To make a comparison, the values of α and β in the weight function are both set to 1.10 in the two algorithms, so that the density value distributions of the undamaged plates are similar. The values of α and β are chosen based on a previous work [21]. The weight function images of monitoring area are shown in Fig. 6. Comparing Fig. 6a, b, the images of the structural weight function are asymmetric for the ramp plate.

In the simulations, Lamb wave signals from sensor network are captured in both the undamaged and the damaged states. The signals are normalized using the peak amplitude of the S_0 mode in the undamaged state. The 53rd sensing path consists of the actuator P12 ($x=0$, $y=150$) and the sensor P05 ($x=450$, $y=150$), and the signal is shown in Fig. 7a. The 53rd sensing path is near the damage ($x=270$, $y=180$). Therefore, there are prominent changes between the undamaged signal and the damaged signal. The fourth sensing path consists of the actuator P01 ($x=0$, $y=0$) and the sensor P09 ($x=150$, $y=450$), which is shown in Fig. 7b. From Fig. 7b, the signals captured in the damaged and undamaged states are almost identical, because the fourth sensing path is away from the damage. 几乎一致

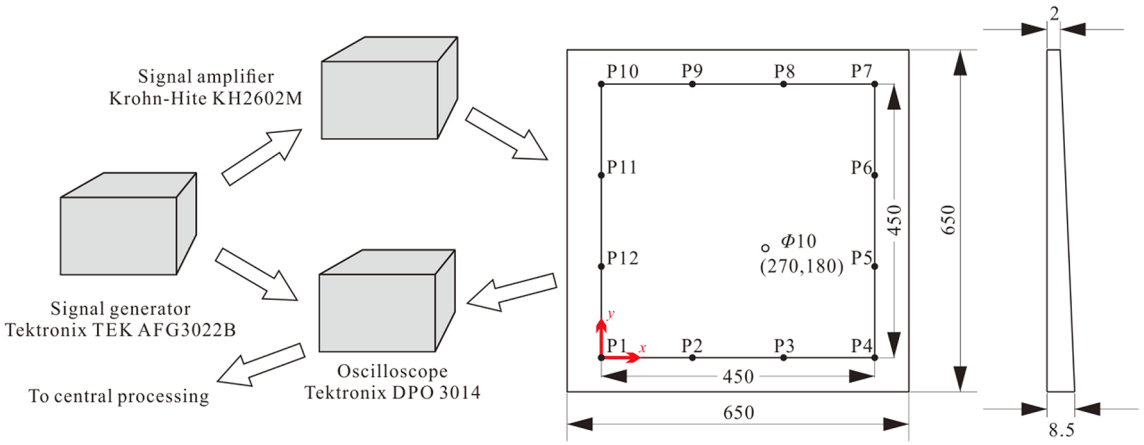

Fig. 5 **a** Schematic diagram of the ramp aluminum plate; **b** sensor network in the monitoring area enclosed by 12 PZTs

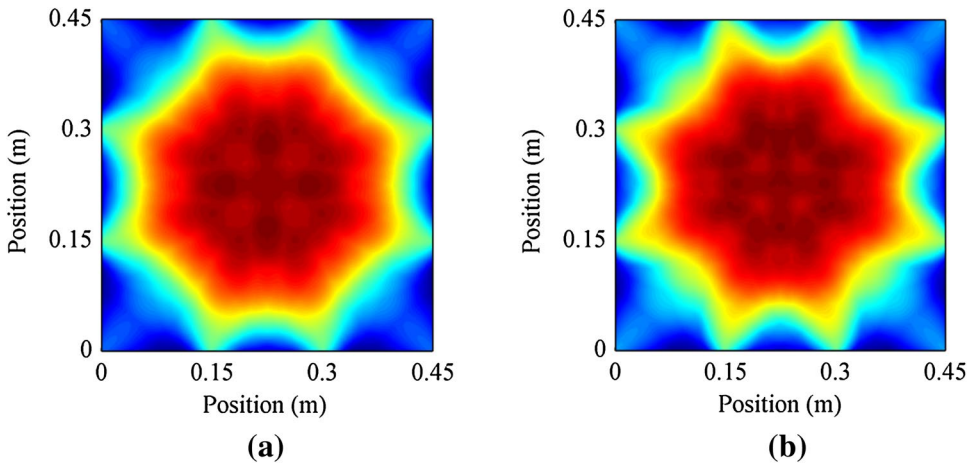

Fig. 6 Images of the weight function in the monitoring area: **a** the linear elliptic weight function for RAPID algorithm; **b** the structural weight function for the RAPID algorithm

The probability-reconstructed images for the RAPID using the linear elliptical weight function and the structural weight function are built up using Eqs. (7)–(8) and Eqs. (11)–(13), as illustrated in Fig. 8a, b, respectively. In the RAPID algorithm, the probability density value in the reconstructed image is proportional to the chance of

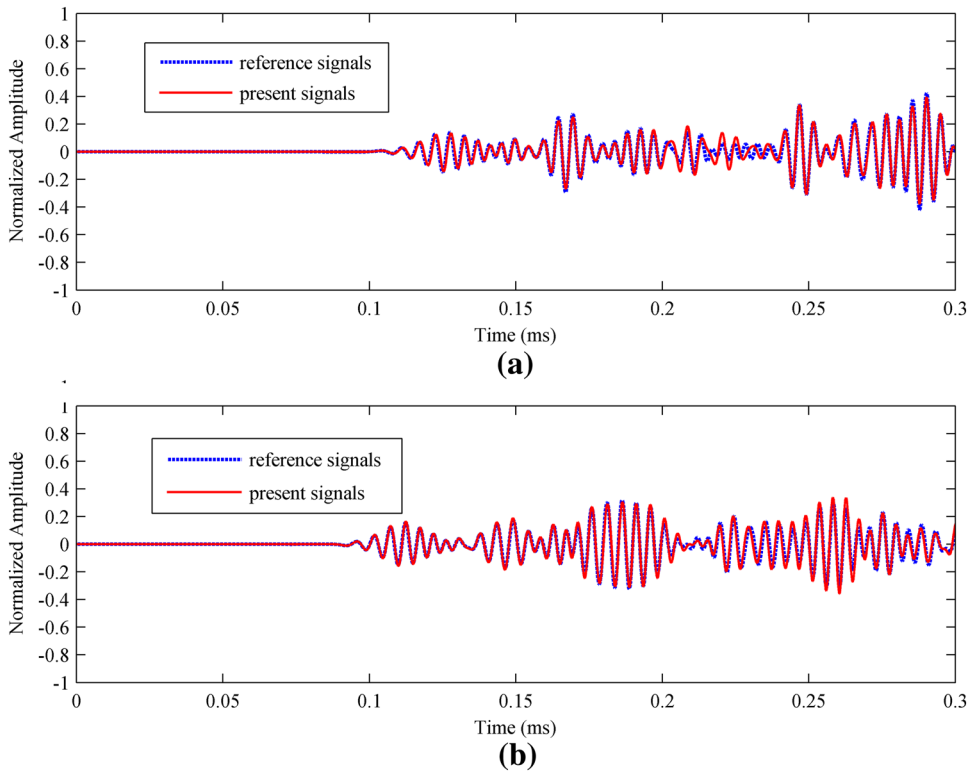

Fig. 7 Captured signals in time domain from different sensing path in the simulation: **a** 53rd consists of P06 and P01; **b** 4th consists of P01 and P05

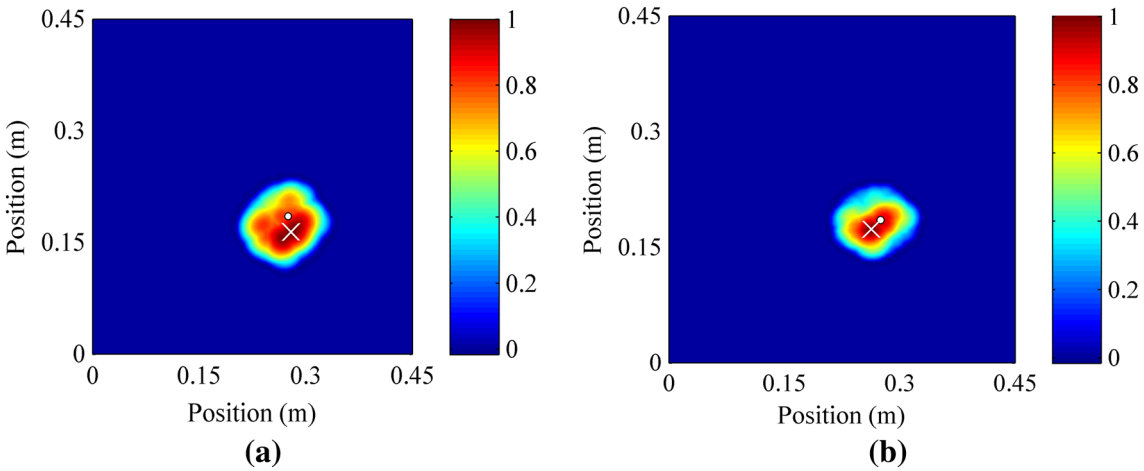

Fig. 8 Probability reconstructed images of simulations **a** using the linear elliptical weight function and **b** using the structural weight function

damage. The highlighted parts represent the positions with probability density greater than 90%, which are the most probable area with damage. The center of the identified damage is marked by a cross symbol, while the actual damage is marked by a black circle scaled at the actual size. Table 2 summarizes the results of the algorithms in terms of the positioning error vectors (the vector from the actual damage to the identified position) and their modules. Comparing the results from Table 2, the improved algorithm provides a smaller positioning error. Therefore,

Table 2 Identification results of simulations using two algorithms (unit:mm)

Name	Conventional algorithm ($\beta = 1.10$)	Improved algorithm ($\alpha = 1.10$)
Center of actual damage	(270, 180)	(270, 180)
Center of identified damage	(279, 164)	(263, 173)
Error module	18.4	9.9
Error vector	(9, −16)	(−7, −7)

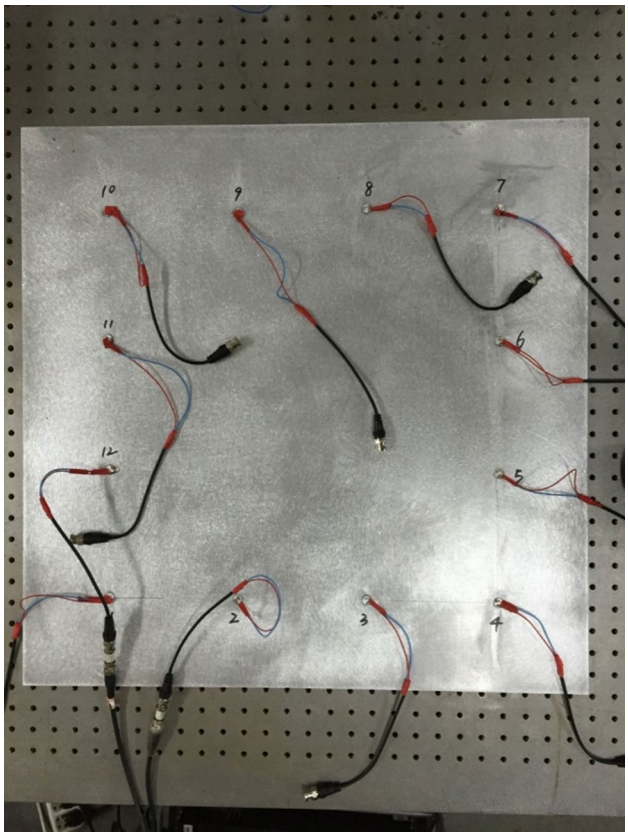

Fig. 9 Experimental setup for damage

Table 3 Material properties of PZT

Density ρ (g/cm^3)	7.8
Charge constant d_{31} (C/N)	-180×10^{-12}
Relative dielectric constant K^T	1750
Frequency constant N_T (Hz m)	2000

the improved algorithm gives a probability image with higher accuracy.

Experiment

The specimen of the ramp plate for experiment is experimentally evaluated shown in Fig. 9, with the same geometry, mechanical properties, and boundary conditions to the finite-element models. The sensor network is developed on the platform with 12 surface-mounted PZT discs (P.I®PIC255) of 10 mm in diameter and 1 mm in thickness, as shown in Fig. 5b. The PZTs are evenly installed on the ramp plate, which enclose a square monitoring area of 450 mm × 450 mm. The material properties of PZTs are shown in Table 3. Generation and acquisition of Lamb waves are fulfilled consisting mainly of an arbitrary signal generator (Tektronix®TEK AFG3022B), a signal power amplifier (Krohn-Hite® KH 7602 M), and an oscilloscope (Tektronix®DPO 3014). In accordance with the simulation, the same excitation signal is selected in both the undamaged and damaged states, which is at a central frequency of 210 kHz. The sampling rate is 100 MHz in the experiments.

Results and Discussion

The results of the experiment show good similarity to that of the FE simulations, but there are still some differences. Lamb wave signals from the sensing network are captured experimentally in both the undamaged and damaged states. Corresponding to the simulations, the signals of 53rd sensing path and 4th sensing path are taken for instance, whose time-domain figures are shown in Fig. 10. The probability-reconstructed images for the two kinks of weight functions are demonstrated in Fig. 11, respectively. Table 4 summarizes the results of the algorithms from the experiment.

Comparing with Table 3, there are several reasons for the differences between the results of tow algorithms. First, ideal conditions set in the simulations cannot be guaranteed in actual experiments. There are other factors affecting the signals, such as the stability of PZTs, the noise of the experimental environment. Second, the hole on the ramp plate is drilled manually. The size and location of the hole are less precise than the one used in the simulation. Moreover, the plate used in the experiment may have been deformed after drilled. Finally, the instrumental error may also affect the experiment results.

Although the errors are unavoidable, the reconstructed images in Fig. 11 still have an accuracy good enough to identify the damage. Table 4 summarizes the identified results of the conventional and improved RAPID algorithms, using the linear weight function and the structural weight function, respectively. The results indicate that the improved algorithm is superior to the conventional one in both probability image accuracy and application scenario range.

Conclusions

The improved reconstruction algorithm for probabilistic inspection of defects based on an active sensor network is developed, especially for structures with non-uniform cross sections. This diagnostic algorithm particularly relies on the weight function put forward in this paper, which corresponds with the top surface function of plates. The algorithm is validated experimentally on a ramp-top surface plate with a 10 mm diameter through-hole defect that an active sensor network containing 12 PZT elements is utilized to generate and capture wave signals in both the

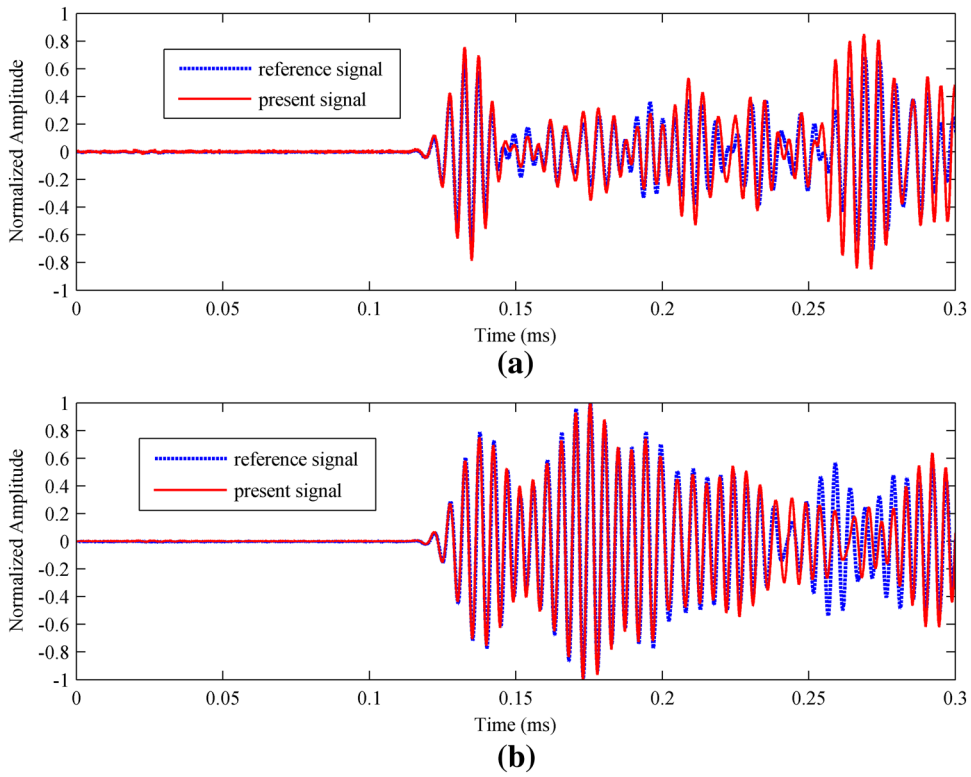

Fig. 10 Captured signals in time domain from different sensing path in the experiment: **a** 53rd consists of P12 and P05; **b** 4th consists of P01 and P09

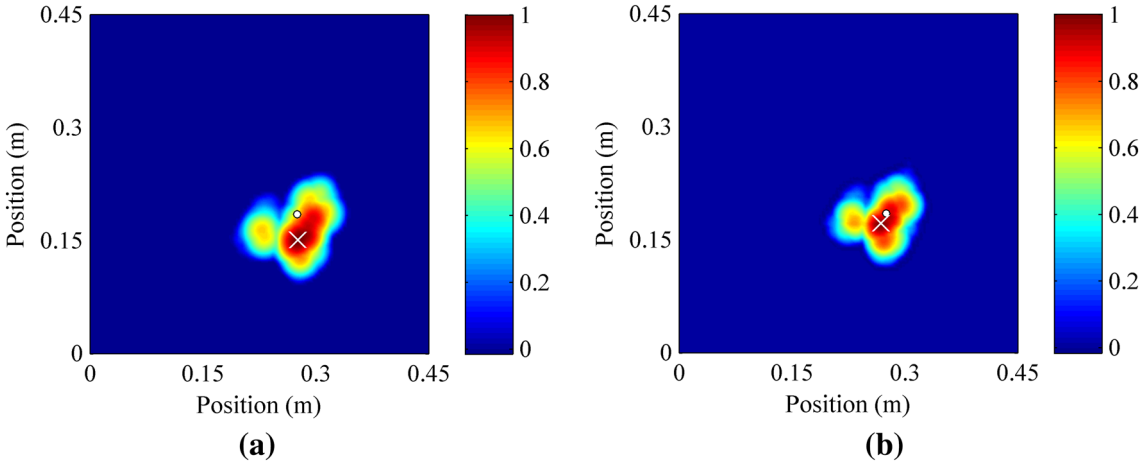

Fig. 11 Reconstructed images of the experiment: **a** using the conventional algorithm and **b** using the improved algorithm

Table 4 Identification results of experiment using two algorithms (units:mm)

Name	Conventional algorithm ($\beta = 1.10$)	Improved algorithm ($\alpha = 1.10$)
Center of actual damage	(270, 180)	(270, 180)
Center of identified damage	(276, 151)	(268, 172)
Error module	29.6	8.2
Error vector	(6, −29)	(−2, −8)

undamaged and damaged states. The high-damage probability area clearly covers or is close to the actual defect in the ramp plate. Compared with the conventional RAPID, the employment of the novel weight function can considerably improve the precision of the localization, and the shape of the high-damage probability area only slightly changes when the scaling parameter is selected appropriately. The results presented in this study indicate that the improved RAPID algorithm is effective.

Acknowledgements The authors would like to gratefully acknowledge the supports received from the National Natural Science Foundation of China (NSFC Nos. 11372179 and 51405291) and Program for New Century Excellent Talents in University (NCET-13-0363).

References

1. Su Z, Ye L (2009) Identification of damage using lamb waves: from fundamentals to applications. Lecture notes in applied and computational mechanics, vol 48. Springer, London
2. Giurgiutiu V (2005) Tuned lamb wave excitation and detection with piezoelectric wafer active sensors for structural health monitoring. J Intell Mater Syst Struct 16:291–305
3. Leonard KR, Hinders MK (2005) Lamb wave tomography of pipe-like structures. Ultrasonics 43:574–583
4. Jansena DP, Hutchinsb D (1992) Immersion tomography using Rayleigh and Lamb waves. Ultrasonics 9:245–254
5. Giurgiutiu V, Bao J (2004) Embedded-ultrasonics structural radar for in situ structural health monitoring of thin-wall structures. Struct. Heal. Monit. 3:121–140
6. Lin X, Yuan FG (2001) Damage detection of a plate using migration technique. J Intell Mater Syst Struct 12:469–482
7. Rose JL (1999) Ultrasonic waves in solid medias
8. Rama Rao GV, Davis TT, Sreekala R, Gopalakrishnan N, Iyer N, Lakshmanan N (2015) Damage identification through wave propagation and vibration based methodology for an axial structural element. J Vib Eng Technol 3:383–399
9. Hay TR, Royer RL, Gao H, Zhao X, Rose JL (2006) A comparison of embedded sensor Lamb wave ultrasonic tomography approaches for material loss detection. Smart Mater Struct 15:946–951
10. Zhao X et al (2007) Active health monitoring of an aircraft wing with embedded piezoelectric sensor/actuator network: I. Defect detection, localization and growth monitoring. Smart Mater Struct 16:1208–1217
11. Zhao X et al (2007) Active health monitoring of an aircraft wing with an embedded piezoelectric sensor/actuator network: II. Wireless approaches. Smart Mater Struct 16:1218–1225
12. Zhao X, Royer RL, Owens SE, Rose JL (2011) Ultrasonic Lamb wave tomography in structural health monitoring. Smart Mater Struct 20:105002
13. Koduru JP, Rose JL (2013) Mode controlled guided wave tomography using annular array transducers for SHM of water loaded plate like structures. Smart Mater Struct 22:125021
14. Zhang M (2015) Numerical investigation of structural damage detection. J Vib Eng Technol 3:2015
15. Wang D, Ye L, Lu Y (2009) A probabilistic diagnostic algorithm for identification of multiple notches using digital damage fingerprints (DDFs). J Intell Mater Syst Struct 20:1439–1450
16. Wang D et al (2010) Probabilistic damage identification based on correlation analysis using guided wave signals in aluminum plates. Struct Heal Monit Int J 9:133–144
17. Wang D, Ye L, Lu Y, Li F (2010) A damage diagnostic imaging algorithm based on the quantitative comparison of Lamb wave signals. Smart Mater Struct 19:065008
18. Sheen B, Cho Y (2012) A study on quantitative lamb wave tomogram via modified RAPID algorithm with shape factor optimization. Int J Precis Eng Manuf 13:671–677
19. Wu Z, Liu K, Wang Y, Zheng Y (2014) Validation and evaluation of damage identification using probability-based diagnostic imaging on a stiffened composite panel. J Intell Mater Syst Struct. https://doi.org/10.1177/1045389X14549873
20. Gao D, Wang Y, Wu Z, Rahim G, Bai S (2014) Design of a sensor network for structural health monitoring of a full-scale composite horizontal tail. Smart Mater Struct 23:055011
21. Zeng L, Lin J, Hua J, Shi W (2013) Interference resisting design for guided wave tomography. Smart Mater Struct 22:055017
22. Cho Y (2000) Estimation of ultrasonic guided wave mode conversion in a plate with thickness variation. IEEE Trans Ultrason Ferroelectr Freq Control 47:591–603
23. El-Kettani ME-C, Luppé F, Guillet A (2004) Guided waves in a plate with linearly varying thickness: experimental and numerical results. Ultrasonics 42:807–812
24. Marical P, El-Kettani ME, Predoi MV (2007) Guided waves in elastic plates with Gaussian section variation: experimental and numerical results. Ultrasonics 47:1–9